Karakoc, Alp; Santaoja, Kari; Freund, Jouni

Simulation experiments on the effective in-plane compliance of the honeycomb materials

Published in:
Composite Structures

DOI:
10.1016/j.compstruct.2012.09.021

Published: 01/01/2013

Document Version
Peer-reviewed accepted author manuscript, also known as Final accepted manuscript or Post-print

SIMULATION EXPERIMENTS ON THE EFFECTIVE IN-PLANE COMPLIANCE OF THE HONEYCOMB MATERIALS

Alp Karakoç *, Kari Santaoja, Jouni Freund

Aalto University, School of Engineering, Department of Applied Mechanics, P.O.BOX 14300, FI-00076 AALTO, FINLAND

ABSTRACT

A statistical simulation model is presented to compute the effective in-plane compliance matrices of the honeycomb materials. The present model is explained in three stages: the micromechanical model, simulation experiments under external loading and boundary conditions, and the analysis of the experiment results. In the micromechanical model, mean values of the geometrical and mechanical parameters and variations related to cell wall height and thickness are used in order to mimic the actual materials in the virtual environment. Simulation experiments are performed on these replicated materials under the assumption of linear elasticity. The effect of solution artefacts near the boundary domain is controlled by defining a measurement domain where the strain and stress fields are assumed to be constant. The simulation results for this domain are processed with transformation and the least squares minimization to obtain the effective in-plane elastic parameters. In this context, two case studies are conducted. The first case study aims at understanding the influences of the cell geometry and aforementioned variations on the linear elastic material behavior. Meanwhile, the scope of the second case study is to validate the proposed model by comparing the simulation results with the measurements conducted on Nomex® honeycomb materials by the authors.

Keywords: Compliance, honeycomb, micromechanical, linear elasticity, cell wall, Nomex®.

*Corresponding author. Tel: +358 470 23442.
Email address: alp.karakoc@aalto.fi (Alp Karakoç).

1. INTRODUCTION

Honeycomb cores are extensively used in different structural applications such as aviation and automotive industries due to their high stiffness-to-weight ratios. Various analytical techniques and numerical analysis methods have been developed in order to predict in- and out-of-plane mechanical properties of these structures. In many analytical studies, predictions of in-plane core properties have been limited to the assumptions of regular cell geometry and constant mechanical properties. The approaches are mainly based on the bending deformation of inclined walls of a hexagonal unit cell modeled as fixed end-guided end beam [1, 2] , while the axial deformation of the vertical walls is neglected due to its minor effect on slender honeycomb cell walls [3, 4]. In addition to these modeling approaches, honeycomb materials contain natural variations in their microstructures which can affect the stiffness and strength properties. The effective in-plane elastic and plastic material behaviors in the context of the cell wall height variations have been discussed in the literature [5-7]. However, the cell wall thickness variations and the effect of double walls, which is present in most of the commercial honeycomb materials as a result of the production methods shown in Fig. 1, have not been investigated in detail.

In order to complete these missing links in the literature, a statistical simulation model is introduced. The aim of the proposed simulation model is to replicate the actual honeycomb material experiments in the virtual environment and compute the effective in-plane compliance matrices. For the replication, the simulation model takes into account both the mean values for the measured geometrical and mechanical properties of the actual honeycomb materials and the variations related to the cell wall height and thickness. Thereafter, the simulation experiments are performed on the replicated materials under the assumption of linear elasticity. The effect of solution artefacts near the boundary domain is controlled by defining a measurement domain where the strain and stress fields are assumed to be constant. The results for this domain are processed with transformation and the least squares minimization to obtain the effective in-plane elastic parameters.

In this context, two case studies are conducted. The first case study aims at understanding the influences of the cell geometry and aforementioned variations on the linear elastic material behavior. Meanwhile, the scope of the second case study is to validate the proposed model by comparing the simulated effective in-plane compliances with the ones determined through the physical experiments on Nomex® honeycomb materials conducted by the authors [8].

---Preferred position for Fig. 1---

2. METHODOLOGY

2.1. Methodology

In order to calculate the effective in-plane mechanical properties of the honeycomb materials, a micromechanical model has been generated as depicted in Fig. 2. In this model, cell walls are represented as beams, the geometrical and mechanical parameters of which are measured and used in the constitutive equations. Each beam is connected to two of its neighbors through their vertices to form a structural unit. Connection process is restricted with continuity conditions concerning displacements and rotations at vertices and the equilibrium equations of the vertex points. The repetitive translations of the structural units are used to build the honeycomb specimens in the virtual environment. By assigning the uni-axial loading and simply supported boundary conditions, the simulation experiments are conducted to obtain the strain and stress fields on a predetermined measurement domain. Eventually, the analysis of the experiment results culminates in the effective in-plane compliance matrices of the honeycomb materials.

---Preferred position for Fig. 2---

2.2. Theoretical background for the effective in-plane compliance

The elastic behaviour of honeycomb materials has been examined theoretically in various publications. The common approach in these studies follows the assumption of orthotropy which introduces the material WL Cartesian coordinate system [1, 3, 10]. $W-$ and $L-$axes of this coordinate system represent the direction of expansion and the ribbon direction, which is shown in Fig. 3 [9]. Under the assumption of orthotropy, the compliance matrix in the basis of *WL* coordinate system is given as

$$[\underline{\mathbf{C}}] = \begin{bmatrix} 1/E_W & -\nu_{LW}/E_L & 0 \\ -\nu_{WL}/E_W & 1/E_L & 0 \\ 0 & 0 & 1/G_{WL} \end{bmatrix}, \tag{1}$$

where E_W, E_L, G_{WL}, ν_{WL}, and ν_{LW} are the effective elastic moduli, shear modulus and Poisson's ratios, respectively, for which $\nu_{LW}/E_L = \nu_{WL}/E_W$ [11].

---Preferred position for Fig. 3---

From the authors' point of view, a priori assumption of orthotropy should be avoided. Conversely, the compliance calculations should be performed under the assumption of general anisotropic linear elasticity and material classification should be done after the analysis of $[\underline{\mathbf{C}}]$ [12]. In this case, the effective in-plane compliance matrix is given as

$$[\underline{\mathbf{C}}] = \begin{bmatrix} 1/E_W & -\nu_{LW}/E_L & \eta_{WL,W}/E_W \\ -\nu_{WL}/E_W & 1/E_L & \eta_{WL,L}/E_L \\ \eta_{WL,W}/E_W & \eta_{WL,L}/E_L & 1/G_{WL} \end{bmatrix} \tag{2}$$

in which the coefficients of mutual influence $\eta_{WL,W}$, $\eta_{WL,L}$ characterize the coupling between shearing and normal stresses [11].

2.3. Transformation rules for the effective in-plane compliance

In a typical honeycomb material experiment, it is essential to define the material WL coordinate system and the laboratory XY coordinate system as illustrated in Fig. 4. These coordinate systems are used to describe the principle material plane and the experiment plane in the laboratory environment, respectively.

---Preferred position for Fig. 4---

Strain-stress relationship in laboratory XY Cartesian coordinate system is constructed using the conventional Voigt notation

$$\{\mathbf{e}\} = [\mathbf{C}]\{\mathbf{s}\} \tag{3}$$

due to practical difficulties in using high-order tensors [11]. Curly {} and square brackets [] are the component representations of the tensors in the basis of a fixed coordinate system. In Eq. (3), $\{\mathbf{e}\}$ and $\{\mathbf{s}\}$ are the column vector representations for the strain and stress tensors with the assumption of symmetry (e_{mn}=e_{nm} and s_{mn}=s_{nm} for $m, n \in \{X, Y\}$), while $[\mathbf{C}]$ is the square matrix representation for the fourth-order compliance tensor **C**. Here, it should be noted that $[\mathbf{C}]$ and $[\underline{\mathbf{C}}]$ denote the compliance in the basis of XY and WL coordinate systems, respectively. Then, Eq. (3) can be represented in the component form as

$$\begin{Bmatrix} e_{XX} \\ e_{YY} \\ 2e_{XY} \end{Bmatrix} = \begin{bmatrix} C_{11} & C_{12} & C_{16} \\ C_{21} & C_{22} & C_{26} \\ C_{16} & C_{26} & C_{66} \end{bmatrix} \begin{Bmatrix} s_{XX} \\ s_{YY} \\ s_{XY} \end{Bmatrix} = [\mathbf{T}]^{\mathrm{T}} \begin{bmatrix} \underline{C}_{11} & \underline{C}_{12} & \underline{C}_{16} \\ \underline{C}_{21} & \underline{C}_{22} & \underline{C}_{26} \\ \underline{C}_{16} & \underline{C}_{26} & \underline{C}_{66} \end{bmatrix} [\mathbf{T}] \begin{Bmatrix} s_{XX} \\ s_{YY} \\ s_{XY} \end{Bmatrix} \tag{4}$$

in which the compliance symmetry is taken into account. Hence, the number of independent parameters reduces to 6 [14]. In Eq. (4), superscript T denotes the matrix transpose and $[\mathbf{T}]$ is the orthogonal transformation matrix. According to [11],

$$[\mathbf{T}] = \begin{bmatrix} \cos^2\varphi & \sin^2\varphi & 2\sin\varphi\cos\varphi \\ \sin^2\varphi & \cos^2\varphi & -2\sin\varphi\cos\varphi \\ -\sin\varphi\cos\varphi & \sin\varphi\cos\varphi & \cos^2\varphi - \sin^2\varphi \end{bmatrix}, \tag{5}$$

where φ is the counterclockwise orientation angle between $X-$ and $W-$axes as depicted in Fig. 4.

In principle, the components of $[\underline{\mathbf{C}}]$, which are $\underline{C}_{11},..,\underline{C}_{66}$, can be measured by using at least three linearly independent homogeneous stress states $s^i_{XX}, s^i_{YY}, s^i_{XY}$ for $i \in \{1, 2, 3\}$. Assuming that the corresponding strain components $e^i_{XX}, e^i_{YY}, e^i_{XY}$ are measured in some manner,

$$[\underline{\mathbf{C}}] = \left[\begin{array}{c:c:c} e^1_{XX} & e^2_{XX} & e^3_{XX} \\ e^1_{YY} & e^2_{YY} & e^3_{YY} \\ 2e^1_{XY} & 2e^2_{XY} & 2e^3_{XY} \end{array}\right] \left[\begin{array}{c:c:c} s^1_{XX} & s^2_{XX} & s^3_{XX} \\ s^1_{YY} & s^2_{YY} & s^3_{YY} \\ s^1_{XY} & s^2_{XY} & s^3_{XY} \end{array}\right]^{-1}. \tag{6}$$

However, in order to be more precise, specimens should be tested for more than three independent stress states, i.e. different material orientations relative to the loading direction. In this case, the compliance components can be calculated as the minimizer of the least squares function

$$\pi(\underline{C}_{11},..,\underline{C}_{66}) = \sum_{i=1}^{n} \left\| \begin{Bmatrix} e_{XX}^{i} \\ e_{YY}^{i} \\ 2e_{XY}^{i} \end{Bmatrix} - [\mathbf{T}]^{\mathrm{T}} \begin{bmatrix} \underline{C}_{11} & \underline{C}_{12} & \underline{C}_{16} \\ \underline{C}_{21} & \underline{C}_{22} & \underline{C}_{26} \\ \underline{C}_{16} & \underline{C}_{26} & \underline{C}_{66} \end{bmatrix} [\mathbf{T}] \begin{Bmatrix} s_{XX}^{i} \\ s_{YY}^{i} \\ s_{XY}^{i} \end{Bmatrix} \right\|^{2} \tag{7}$$

in which the matrix norm $\| \ \|$ is the Euclidean. For a unique minimizer, i.e. the values of the material parameters, the number of independent equations should be equal to or exceed that of the parameters, which can be achieved with the repetitive measurements on various stress states.

The analysis of the compliance components $\underline{C}_{11},..,\underline{C}_{66}$ in Eq. (7) clarifies the interaction between the shear stresses and normal strains as well as the interaction between the shear stresses and shear strains in the predetermined principal material plane. If there is no interaction between these, the coefficients of mutual influence $\eta_{WL,W}$, $\eta_{WL,L}$ of Eq. (2) are equal to zero and the material can be termed orthotropic. In case that there is interaction, it is recommended to redefine the principal material plane and apply the transformation rules to Eq. (7) with the new angular configuration till the interaction is minimized.

3. MICROMECHANICAL MODEL

In order to calculate the in-plane mechanical properties of the honeycomb material, various studies have been conducted in which the main strategy is based on the continuum models or the micromechanical models. In the continuum models, the heterogeneous medium, e.g. the honeycomb material, is expressed as an equivalent homogeneous medium, where the geometrical and mechanical characteristics of the microscopic heterogeneities are averaged over the representative volume elements [15]. In order to represent the physics of the material accurately, e.g. stress-strain relationship, these volume elements must include large number of microscopic heterogeneities [16]. However, the determination of the convenient volume element size is subjective and can easily lead to errors in understanding the effects of microscopic variations of constituent on macroscopic mechanical properties.

Since the main focus is on the microscopic characteristics, the current micromechanical model represents the honeycomb material as a heterogeneous medium by using a beam network. Hence, direct calculations can be performed to obtain the microscopic mechanical quantities.

3.1. Material element

The material element is a rectangular honeycomb material with the solution domain of $\mathcal{W} \times \mathcal{L}$, where $\mathcal{W}$ and $\mathcal{L}$ denote the core width and length as seen in Fig. 5. The mean independent geometrical parameters of the material are the cell size c, corner angle θ, cell wall height h and thickness t, and core thickness $\mathcal{T}$. In addition, the variations related to the cell wall height $\alpha = h_{\text{stdev}} / h_{\text{mean}}$ and thickness $\beta = t_{\text{stdev}} / t_{\text{mean}}$ are the other independent geometrical parameters, for which the subscripts stdev and mean denote the standard deviation and mean value. The latter two parameters α and β are used to describe the bounds of the geometrical irregularities which are inserted to the material geometry in several steps. In the initial step, the regular geometry is formed with the aforementioned geometrical parameters, where $\alpha = 0$ and $\beta = 0$. In this step, the positions of the cell vertices are extracted and assigned as the centers of discs which have radii of $\Delta h = \alpha h^0$. Here, h^0 is the cell wall height of the regular geometry. Following this, a random point is picked from each disc. These selected points result in different vertex positions (consequently, cell wall heights) than the ones of regular geometry. Similar description is applied to the cell wall thickness, where the random point picking is performed on a line with the offset magnitude $\Delta t = \beta t^0$, instead. Here, t^0 stands for the cell wall thickness of the regular geometry. As a result of these steps, the irregular material geometry is generated which is also illustrated in Fig. 5. In this figure, $\alpha = 0$ and $\beta = 0$ correspond to the regular honeycomb geometry with the corner angle $\theta = 30^\circ$, while $\alpha > 0$ and $\beta > 0$ correspond to an irregular material geometry.

In the laboratory *XY* coordinate system, the solution domain occupied by the specimen is $\Omega = [0, \mathcal{W}] \times [0, \mathcal{L}]$, where $\partial\Omega$ represents the boundary domain.

---Preferred position for Fig. 5---

3.2. Beam equations

In the micromechanical model, the cell walls shown in Fig. 5 are modeled as elastic Bernoulli beams. The material inside the cells is assumed to be softer than that of the cell walls, thus its influence on the mechanical response is neglected. The component form of the equilibrium equations in the beam *xyz*-coordinate system of Fig. 2 is given as

$$\begin{Bmatrix} E_s A u_x'' \\ -E_s I u_y^{(4)} \end{Bmatrix} + \begin{Bmatrix} \underline{f}_x \\ \underline{f}_y \end{Bmatrix} = \begin{Bmatrix} 0 \\ 0 \end{Bmatrix} \tag{8}$$

in which u_x, u_y are the continuous displacements and $\underline{f}_x$, $\underline{f}_y$ are the external load components in the directions of the *x*- and *y*-axes, respectively. The Lagrange's notation is used to denote the derivatives with respect to *x*. The geometrical properties of beam cross sections are the area $A = \mathcal{T}t$ and the second moment of area $I = \mathcal{T}t^3/12$. Elastic modulus E_s is the constant valued material parameter of the problem. The *x*-axis of the *xyz*-coordinate system is assumed to coincide with the neutral axis of the beam.

Solution to Eq. (8) for the cell walls modelled as beams is connected by continuity conditions concerning the displacements and rotations at the vertices and the equilibrium equations of the vertex points.

4. EXPERIMENTS

In the present experimental program, two case studies are conducted. The first case study aims at understanding the influences of the cell geometry and variations related to cell wall height and thickness on the linear elastic material behavior. Meanwhile, the scope of the second case study is to validate the proposed model by comparing the simulated effective in-plane compliances with those of the physical experiments on Nomex® honeycomb materials performed by the authors.

4.1. Design of experiments

The independent parameters of the experiments are the material type, material orientation angle φ between the *WL* and the laboratory *XY* coordinate systems, and the applied load vector $\underline{\vec{F}}$. The material type is described in terms of the cell geometry c, θ, h, t, α and β, core thickness $\mathcal{T}$, and the cell wall elastic modulus E_s. These parameters are assumed to satisfy the cell wall (beam) slenderness $E_s I / E_s A h^2 \ll 1$ so that the cell wall bending is the dominant deformation mechanism [17]. The dependent variable of the experiments is the effective in-plane compliance matrix $[\underline{\mathbf{C}}]$, the computations of which are performed in a measurement domain Ω_{m} under the assumption of constant strain and stress fields.

4.1.1. Investigation on the effects of the geometrical variations

In order to understand the effects of geometrical variations on the effective in-plane compliance, 16 honeycomb samples are formed by using the cell wall height variations $\alpha \in \{0, 0.05, 0.10, 0.15\}$ and thickness variations $\beta \in \{0, 0.05, 0.10, 0.15\}$. The mean geometrical parameters are determined to be $c = 10$ mm, $\mathcal{T} = 7$ mm, $\theta = 30^\circ$, $t/h = 0.023$ and $E_s = 7.9$ GPa. For each sample, 20 specimens are generated and tested.

4.1.2. Validation of the model

In order to mimic the previously performed physical experiments in the virtual environment, the same cell sizes, which are $c \in \{5, 6, 13\}$ mm, and the core thicknesses of $\mathcal{T} \in \{7, 12\}$ mm are used. The samples are generated based on these two parameters, whereas the specimens of each sample are formed using four different orientations $\varphi \in \{0^\circ, 45^\circ, -45^\circ, 90^\circ\}$ relative to the loading direction. The cell wall height and thickness variations α and β of each sample are obtained in average sense by measuring 20 random spots on each actual specimen. The length-to-width ratio (aspect ratio) of the specimens is decided to be two, for which $\mathcal{W} = 150$ mm and $\mathcal{L} = 300$ mm. Here, it is noteworthy that the mean value of the cell wall elastic modulus $E_s = 7.9$ GPa, which was measured through uni-axial tension tests of unit cell structure [8]. By means of the listed geometrical parameters in Table 1, 20 specimens are generated and simulated for each case.

---Preferred position for Table 1---

4.2. Experiments

Simulation experiments on the effective in-plane compliance of Nomex® honeycomb materials are performed with an in-house code written with Mathematica® software package. After assigning the microscopic mechanical properties to the statistically generated material elements, the experiments are carried out under the uni-axial tensile loading and simply supported boundary conditions in the laboratory XY coordinate system. More precisely, the boundary conditions are imposed in the way that the center point of the upper boundary extreme is pinned. The rest of the extreme follows the motion of the center point with the given rigid body constraint. Therefore, only rotation around the XY normal vector is allowed for the upper boundary extreme. The similar constraints are valid for the lower boundary extreme except that the translation along Y-axis is also allowed. These set constraints aim at simply supported boundary conditions which minimize the effects of bending moments and shear at the boundary extremes. Hence, the near-ideal shape deformation can be succeeded.

As illustrated in Fig. 6, the uni-axial tensile load $\underline{F}$ with an increment of 1 N is applied on the control point located at the lower boundary domain $\partial\Omega$. In order to ensure the linear elasticity assumption, the upper limit for $\underline{F}$ is fixed as 6 N, which was obtained from the previous physical experiments [8].

In order to calculate the vertex displacements as the function of $\underline{F}$, the set of equilibrium equations given in Eq. (8) is solved for the solution domain Ω. The effect of solution artefacts near the boundaries is controlled by defining a measurement domain Ω_{m} which is smaller than the solution domain Ω. The strain and stress fields are assumed to be constant inside Ω_{m}. Hence, the determination of the effective in-plane compliance is performed solely inside this domain.

---Preferred position for Fig. 6---

5. ANALYSIS

5.1. Strain analysis

In order to measure the displacements for each load increment f, 15 tracing points (vertices) $\left(X_i, Y_i\right)$ are selected inside Ω_{m} as seen in Fig. 6. The displacements of these tracing points are calculated as

$$\begin{Bmatrix} u_{Xi}^f \\ u_{Yi}^f \end{Bmatrix} = \begin{Bmatrix} X_i^{f+1} - X_i^f \\ Y_i^{f+1} - Y_i^f \end{Bmatrix} \tag{9}$$

in which u_X, u_Y are the displacement components in the directions of *X*- and *Y*-axes, respectively. The left hand side components of Eq. (9) are considered as the values of continuous linear displacement field $\vec{u}^f$, the component form of which is expressed as

$$\begin{Bmatrix} u_X^f \\ u_Y^f \end{Bmatrix} = \begin{bmatrix} p_1^f & p_2^f & p_3^f \\ p_4^f & p_5^f & p_6^f \end{bmatrix} \begin{Bmatrix} 1 \\ X \\ Y \end{Bmatrix}. \tag{10}$$

The polynomial coefficients p_j^f for $j \in \{1, 2, .., 6\}$ in Eq. (10) are the minimizers of the least squares function

$$\pi(p_1^f, p_2^f, \ldots) = \sum_{i=1}^{n} \left\| \begin{Bmatrix} u_{Xi}^f \\ u_{Yi}^f \end{Bmatrix} - \begin{bmatrix} p_1^f & p_2^f & p_3^f \\ p_4^f & p_5^f & p_6^f \end{bmatrix} \begin{Bmatrix} 1 \\ X_i^f \\ Y_i^f \end{Bmatrix} \right\|^2 \tag{11}$$

in which the sum is over *n* tracing points. In the current analysis, the rigid body rotation inside Ω_{m} is excluded. Hence, the symmetric part of the deformation gradient gives the linear strain $\boldsymbol{\varepsilon}$, the components of which are

$$\begin{Bmatrix} \varepsilon_{XX} \\ \varepsilon_{YY} \\ 2\varepsilon_{XY} \end{Bmatrix} = \begin{Bmatrix} \partial u_X / \partial X \\ \partial u_Y / \partial Y \\ \partial u_X / \partial Y + \partial u_Y / \partial X \end{Bmatrix}. \tag{12}$$

5.2. Stress analysis

For the constitutive modelling, the stress tensor should be selected energy conjugate to the strain tensor $\boldsymbol{\varepsilon}$. This is satisfied with the Cauchy stress tensor $\boldsymbol{\sigma}$ which can be expressed in terms of infinitesimal load vector $d\vec{F}$, unit area da and unit surface normals $\vec{n}^1$, $\vec{n}^2$ in the deformed configuration of Fig. 7. Hence,

$$\begin{Bmatrix} dF_X^i \\ dF_Y^i \end{Bmatrix} = \begin{bmatrix} \sigma_{XX} & \sigma_{YX} \\ \sigma_{XY} & \sigma_{YY} \end{bmatrix} \begin{Bmatrix} n_X^i \\ n_Y^i \end{Bmatrix} da, \; i \in \{1, 2\}. \tag{13}$$

The calculations are carried out for two unit surfaces of the infinitesimal element in order to solve the four unknown components of $\boldsymbol{\sigma}$. Eventually, the components of $\boldsymbol{\varepsilon}$ and $\boldsymbol{\sigma}$ are replaced with $\mathbf{e}$ and $\mathbf{s}$ of Eq. (3) for calculating the effective in-plane compliance.

---Preferred position for Fig. 7---

6. RESULTS AND DISCUSSIONS

In the first part of this section, the effects of geometrical variations related to the cell wall height and thickness α, β on the effective in-plane compliance are analyzed. The second and third parts present the comparison between the physical and simulation experiments in order to investigate the effects of mean geometrical parameters $c, t/h, \theta, \mathcal{T}$ and validate the proposed simulation model.

6.1. Effects of the geometrical variations on the effective in-plane compliance

In order to understand the effects of geometrical variations on the effective in-plane compliance, 16 honeycomb samples are formed with different cell wall height and thickness variations. The simulation results of these samples are given in Table 2 which lists the non-dimensional elastic parameters for the comparison.

---Preferred position for Table 2---

The results of Table 2 and Fig. 8 indicate that the effective in-plane elastic moduli E_W, E_L, and shear modulus G_{WL} increase with increasing cell wall thickness variation β.

This can be attributed to the superiority of the thicker cell walls over the thinner ones. Since the uniform distribution is used for the cell wall thickness, it is expected to have a uniform distribution for the bending stiffness of the cell walls. However, it appears that the thick cell walls counteract the weakening effect of the thin ones and contribute to the effective in-plane moduli. Although further effort is put into understanding the influence of β on the effective Poisson's ratios v_{WL}, v_{LW}, the relationship between these is found to be weak.

---Preferred position for Fig. 8---

Similarly, the analysis of cell wall height variation α reveals that irregular cell shapes contribute to E_W, E_L, and G_{WL}, while the influence on v_{WL}, v_{LW} is insignificant. As seen in Fig. 5, in addition to the hexagonal cells, formation of polyhedrons, such as tetragons and pentagons, are more likely with increasing α. This topological change influences the cell wall deformation mechanisms and hence the stiffness. Although the cell wall bending is the dominant deformation mechanism for the hexagonal topologies, the less-sided topologies are subject to stretch-dominated deformation due to increasing rigidity [18, 19]. Hence, the stiffness of these less-sided topologies is higher than that of the hexagons, which results in higher effective in-plane elastic moduli [20, 21]. As seen in Fig. 9, especially for higher cell wall thickness variation β, this outcome becomes more evident.

---Preferred position for Fig. 9---

6.2. Validation of the model

6.2.1. Effects of mean geometrical parameters on the effective in-plane compliance

The results of both physical and simulation experiments are listed in Table 3 in order to (a) investigate the effects of mean geometrical parameters on the effective in-plane compliance and (b) validate the proposed statistical simulation model. For this purpose, six different samples are formed by using three different cell sizes $c \in \{5, 6, 13\}$ mm, and two different core thicknesses of $\mathcal{T} \in \{7, 12\}$ mm.

---Preferred position for Table 3---

The first notable outcomes of both physical and simulation experiments are the coefficients of mutual influence $\eta_{WL,W}$ and $\eta_{WL,L}$ which are used to classify the material. If these are equal to zero in the planar case, material is termed orthotropic, which represents a particular type of anisotropy. As seen in Table 3, $\eta_{WL,W}$ and $\eta_{WL,L}$ are close to zero, which means that the tested honeycomb cores can also be classified as orthotropic materials. The second important outcome of the investigation is the dominant effect of corner angle θ on the elastic parameters. The comparison between the samples shows that the relationship between E_W and E_L are based on the θ value, which is mainly due to the contribution of the inclined cell walls [4]. When θ is greater than 30°, more material is oriented along the $L-$axis. Therefore, the material becomes stiffer along $L-$axis and softer along $W-$axis. As a result, $E_W < E_L$ for $\theta > 30^\circ$ and $E_W > E_L$ for $\theta < 30^\circ$. The tabulated results also demonstrate that the cell wall thickness-to-height ratio t/h has directly proportional effect on the elastic parameters. For example, the comparison of the samples S-13-7 and S-13-12, which have almost the same corner angle $\theta = 32^\circ$, shows that when t/h decreases, all effective in-plane moduli decrease. This is due to the increasing slenderness of the cell walls and thus the decreasing strength [1, 22]. Similarly, efforts are also put into understanding the effect of $\mathcal{T}$ by comparing the same cell-sized samples with different core thicknesses, e.g. S-5-7 and S-5-12. However, its effect seems trivial compared to the dominant effects of θ and t/h.

6.2.2. The comparison between the physical and simulation experiments

The results of Table 3 shows that the maximum relative error between the physical and simulation experiments is 19.0% for E_W of the sample S-13-12, while the minimum relative error is 1.1% for v_{WL} of the sample S-5-12. The relative error is possibly due to the artefacts originated from the boundary conditions in the physical experiments. Although it is assumed in the simulation experiments that the rotation around XY normal vector is allowed at the upper boundary extreme, the existence of contact friction on the upper pinned support is likely and restrains the rotation in the actual setup. This can alter the configuration from the simply supported boundary conditions and give rise to the transverse strains on the boundaries. Another reason for this error term can be the relative eccentricity of the upper and lower supports in the physical experiments resulting in anomalous measurement errors [23].

The strain legend bars in Fig. 10 indicate that the strain measures of both physical and simulation experiments are in good agreement. However, the visual comparison of the same figure reveals that the measurement domain is affected by the aforementioned artefacts. Especially, the shear strain field in Fig. 10f is questionable in this sense. By confining the measurement domain Ω_m to a smaller region in the middle section, the artefacts due to the boundaries can be prevented and the assumption of constant strain field is acceptable. However, the details of the structure should be taken into consideration in defining the domain size [24].

---Preferred position for Fig. 10---

7. CONCLUSIONS

The present study introduces a statistical simulation model for computing the effective in-plane compliance matrices of the honeycomb materials. The proposed simulation model is designed so that once the actual material geometry is described in a statistical manner; it can be virtually replicated and tested under the given loading and boundary conditions.

The model is firstly used for understanding the effects of geometrical variations related to the cell wall height and thickness α, β on the effective in-plane compliance. This study indicates that both α and β contribute to the effective in-plane elastic moduli E_W, E_L, and shear modulus G_{WL}. However, their influences on the Poisson's ratios v_{WL}, v_{LW} are negligible.

Following this study, another case study is performed to investigate the effects of mean geometrical parameters $c, t/h, \theta, \mathcal{T}$ and validate the proposed simulation model. The results of the simulation experiments are compared with those of the physical experiments on Nomex® honeycomb materials. The comparative investigation for the geometrical parameters of the honeycomb materials shows that the corner angle θ and the cell wall thickness-to-height ratio t/h have dominant effects on the effective in-plane moduli. However, the effect of core thickness $\mathcal{T}$ is trivial compared to the effects of θ and t/h.

The model predicts the effective in-plane elastic parameters within the relative error range of $1.1\% - 19\%$. The reason of the relative error between the physical and simulation experiments is supposed to be the artefacts originated from the boundary conditions in the physical experiments. Violation of the simply supported boundary conditions and the existence of eccentricity between upper and lower supports can alter the configuration. In this respect, consideration of these issues in the simulation experiments or refinement of the physical experiment setup can increase the accuracy of the results.

ACKNOWLEDGEMENTS

The authors gratefully acknowledge the financial support of Multidisciplinary Institute of Digitalisation and Energy (MIDE) through Energy Efficient Wood Processing and Machining Project (E-wood) at Aalto University and the Ministry of Education of Finland through the National Graduate School in Engineering Mechanics. Discussions and proofreading by Ms. Linda Molin are deeply appreciated.

REFERENCES

[1] Gibson LJ, Ashby MF. Cellular solids, structure and properties. Cambridge: Cambridge University Press; 1999.

[2] Abd El-Sayed FK, Jones R, Burgess IW. A theoretical approach to deformation of honeycomb based composite materials. Composites 1979; 10: 209-214.

[3] Masters IG, Evans KE. Models for the elastic deformation of honeycombs. Composite Structures 1996; 35: 403-422.

[4] Balawi S, Abot JL. A refined model for the effective in-plane elastic moduli of hexagonal honeycombs, Composite Structures 2008; 84: 147-158.

[5] Silva MJ, Gibson LJ. The effects of non-periodic microstructure and defects on the compressive strength of two-dimensional cellular solids. International Journal of Mechanical Sciences 1997; 39: 549-563.

[6] Zhu HX, Hobdell JR, Windle AH. Effects of cell irregularity on the elastic properties of 2D Voronoi honeycombs. Journal of the Mechanics and Physics of Solids 2001; 49: 857-870.

[7] Ajdari A, Nayeb-Hashemi H, Canavan P, Warner G. Effect of defects on elastic–plastic behavior of cellular materials. Materials Science and Engineering: A 2008; 487: 558-567.

[8] Karakoç A, Freund J. Experimental studies on mechanical properties of cellular structures using Nomex® honeycomb cores. Composite Structures 2012; 94: 2017-2024.

[9] Hexcel product data sheet:
(Available online: http://www.hexcel.com/Resources/Honeycomb-Data-Sheets (Last check: May 2012)).

[10] Chen DH, Horii H, Ozaki S. Analysis of in-plane elastic modulus for a hexagonal honeycomb core: Analysis of Young's modulus and shear modulus. Journal of

Computational Science and Technology 2009; 3: 1-12.

[11] Jones RM. Mechanics of Composite Materials. Washington, D.C.: McGraw-Hill Book Company; 1975.

[12] Felippa CA, Onate E. Stress, strain and energy splittings for anisotropic elastic solids under volumetric constraints. Computers and Structures 2003; 81: 1343-1357.

[13] Belytschko T, Liu WK,Moran B. Nonlinear Finite elements for Continua and Structures, 1st Ed. New York: Wiley-Sons; 2000.

[14] Kaw AK. Mechanics of Composite Materials, 2nd Ed. Boca Raton: Taylor-Francis Group; 2006.

[15] Landis E, Vasic S, Davids WG, Parrod P. Coupled experiments and simulations of microstructural damage in wood. Experimental Mechanics 2002; 42: 389-394.

[16] Nemat-Nasser S, Hori M. Micromechanics: Overall Properties of Heterogeneous Materials, 2nd Ed. North Holland; 1999.

[17] Karakoç A, Freund J. Effect of geometrical features and scale on failure initiation of wood like cellular material. Proceedings of the 10th Finnish mechanics days; 2009: 534-540.

[18] Deshpande VS, Ashby MF, Fleck NA, Foam topology: bending versus stretching dominated architectures, Acta Materialia 2001; 49: 1035-1040.

[19] Vural M, Alkhader M. Mechanical response of cellular solids: Role of cellular topology and microstructural irregularity. International Journal of Engineering Science 2008; 46: 1035–1051.

[20] Li K, Gao XL, Subhash G. Effects of cell shape and strut cross-sectional area variations on the elastic properties of three-dimensional open-cell foams. Journal of the Mechanics and Physics of Solids 2006; 54: 783-806.

[21] Wang AJ, Kumar RS, McDowell DL. Mechanical Behavior of Extruded Prismatic Cellular Metals. Mechanics of Advanced Materials and Structures 2005; 12: 185–200.

[22] Balawi S, Abot JL. The effect of honeycomb relative density on its effective in-plane elastic moduli: An experimental study. Composite Structures 2008; 84: 293-299.

, Morton J. Determination of G12 by means of the off-axis tension test: Part I: Review of gripping systems and correction factors. Composites Part A: Applied Science and Manufacturing 2002; 33: 87-100.

[24] Takano N, Zako M, Fujitsu R, Nishiyabu K. Study on large deformation characteristics of knitted fabric reinforced thermoplastic composites at forming temperature by digital image-based strain measurement technique. Composites Science and Technology 2004; 64: 2153-2163.

Table 1: Mean values of the measured geometrical parameters of the Nomex® samples. Here, $\alpha = h_{\text{stdev}}/h_{\text{mean}}$ and $\beta = t_{\text{stdev}}/t_{\text{mean}}$.

Sample	c (mm)	$\mathcal{T}$ (mm)	θ ($^\circ$)	h (mm)	t (mm)	α	β
S-5-7	5	7	32	2.5	0.05	0.06	0.06
S-5-12	5	12	34	2.5	0.05	0.04	0.09
S-6-7	6	7	26	3.2	0.06	0.03	0.04
S-6-12	6	12	28	3.2	0.06	0.03	0.03
S-13-7	13	7	32	6.6	0.13	0.03	0.01
S-13-12	13	12	32	6.8	0.13	0.03	0.01

Table 2: Non-dimensional effective in-plane elastic parameters for the honeycomb samples with the mean values $c = 10$ mm, $\mathcal{T} = 7$ mm, $\theta = 30^{\circ}$ and $t/h = 0.023$. Only the bending effect is included. Here, $E_W^* = E_W / \underline{E}$, $E_L^* = E_L / \underline{E}$, $G_{WL}^* = G_{WL} / \underline{E}$, for which $\underline{E} = E_s \left(t/h\right)^3$ and $E_s = 7.9$ GPa is the mean value of the cell wall elastic modulus.

Sample	α	β	E_W^*	E_L^*	G_{WL}^*	ν_{WL}	ν_{LW}	$\eta_{WL,W}$	$\eta_{WL,L}$
1	0	0	1.83	2.02	1.40	0.90	1.00	-0.012	-0.013
2	0.05	0	1.83	2.03	1.40	0.90	1.00	-0.011	0.015
3	0.10	0	1.87	2.05	1.40	0.88	0.97	-0.026	0.016
4	0.15	0	2.00	2.08	1.42	0.91	0.95	-0.024	0.030
5	0	0.05	2.06	2.05	1.44	0.88	0.87	-0.010	0.011
6	0.05	0.05	2.23	2.19	1.55	0.88	0.87	-0.009	0.009
7	0.10	0.05	2.39	2.44	1.69	0.87	0.89	-0.009	0.012
8	0.15	0.05	2.71	2.86	1.88	0.85	0.90	-0.006	0.012
9	0	0.10	2.28	2.26	1.43	0.84	0.83	-0.002	0.011
10	0.05	0.10	2.66	2.64	1.63	0.85	0.84	-0.002	0.014
11	0.10	0.10	3.07	3.06	1.81	0.85	0.85	-0.002	0.014
12	0.15	0.10	3.41	3.46	2.12	0.82	0.83	-0.001	0.016
13	0	0.15	2.40	2.50	1.58	0.81	0.84	-0.004	0.030
14	0.05	0.15	2.75	2.85	1.82	0.81	0.84	-0.003	0.029
15	0.10	0.15	3.20	3.26	2.20	0.83	0.84	0.008	0.070
16	0.15	0.15	3.74	3.86	2.60	0.82	0.85	0.004	0.035

Table 3: Results of the physical and simulation experiments on Nomex® honeycomb samples. Prefix Vi- stands for the simulation samples and the series without suffixes are the samples used in the previous physical experiments performed by the authors.

Sample	t/h	θ	α	β	E_W (kPa)	E_L (kPa)	G_{WL} (kPa)	ν_{WL}	ν_{LW}	$\eta_{WL,W}$	$\eta_{WL,L}$
S-5-7	0.02	32°	0.06	0.06	121.0	158.5	92.6	1.12	1.47	-0.019	0.103
Vi-S-5-7					113.9	152.2	87.3	1.01	1.35	-0.076	0.023
S-5-12	0.02	34°	0.04	0.09	105.8	159.8	98.3	0.97	1.47	0.049	-0.004
Vi-S-5-12					119.3	148.3	94.6	0.98	1.22	-0.018	-0.115
S-6-7	0.0188	26°	0.03	0.04	171.9	118.0	64.3	1.31	0.89	0.048	-0.077
Vi-S-6-7					161.2	113.9	58.1	1.23	0.87	0.061	0.056
S-6-12	0.0188	28°	0.03	0.03	150.0	105.7	71.4	1.29	0.91	0.104	0.075
Vi-S-6-12					141.6	116.4	66.9	1.17	0.96	-0.022	0.081
S-13-7	0.0197	32°	0.03	0.01	122.9	154.2	91.9	1.26	1.58	-0.073	0.069
Vi-S-13-7					126.0	150.2	80.3	1.08	1.28	0.056	0.059
S-13-12	0.0191	32°	0.03	0.01	96.5	128.2	84.6	0.91	1.21	-0.004	-0.024
Vi-S-13-12					114.9	136.8	76.6	0.94	1.13	0.044	-0.038

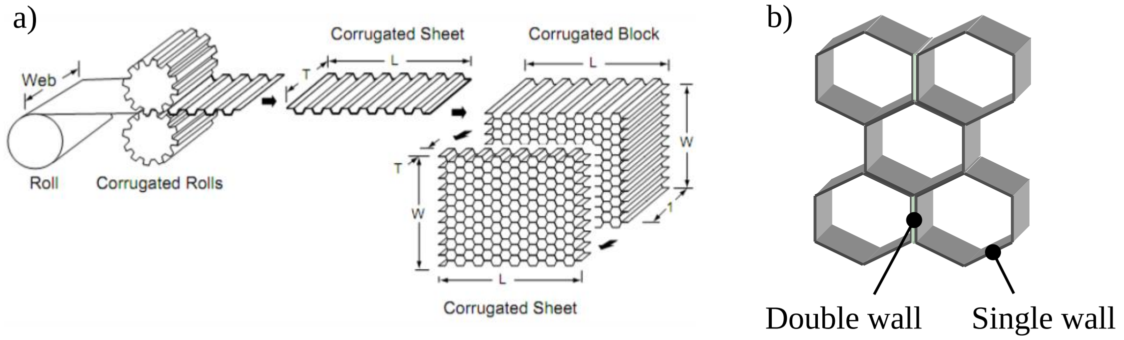

Figure 1: Commercial honeycomb cores: a) production process and b) representative structure with single and double walls [9].

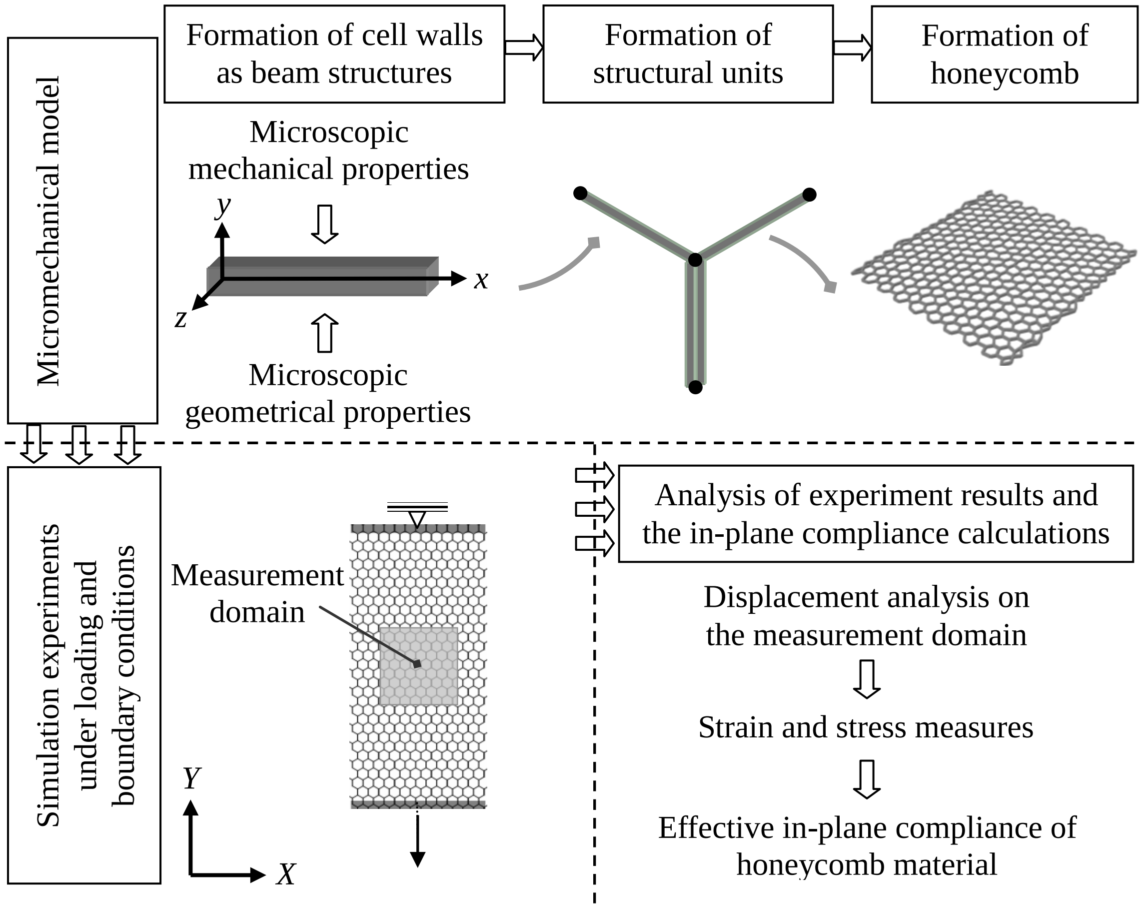

Figure 2: Workflow of the study.

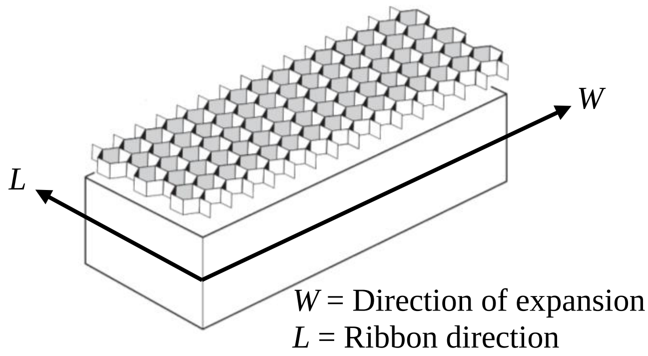

Figure 3: Honeycomb material directions provided in the data sheet [9].

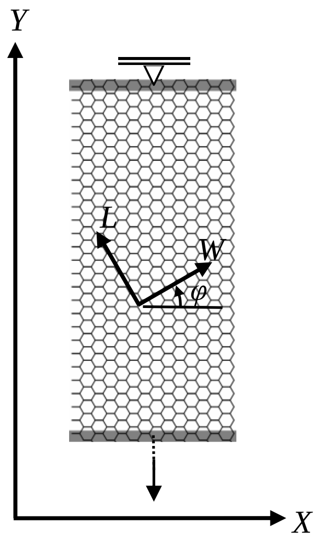

Figure 4: Representation of the material WL coordinate system and the laboratory XY coordinate system. Here, φ is the counterclockwise orientation angle between $X-$ and $W-$axes.

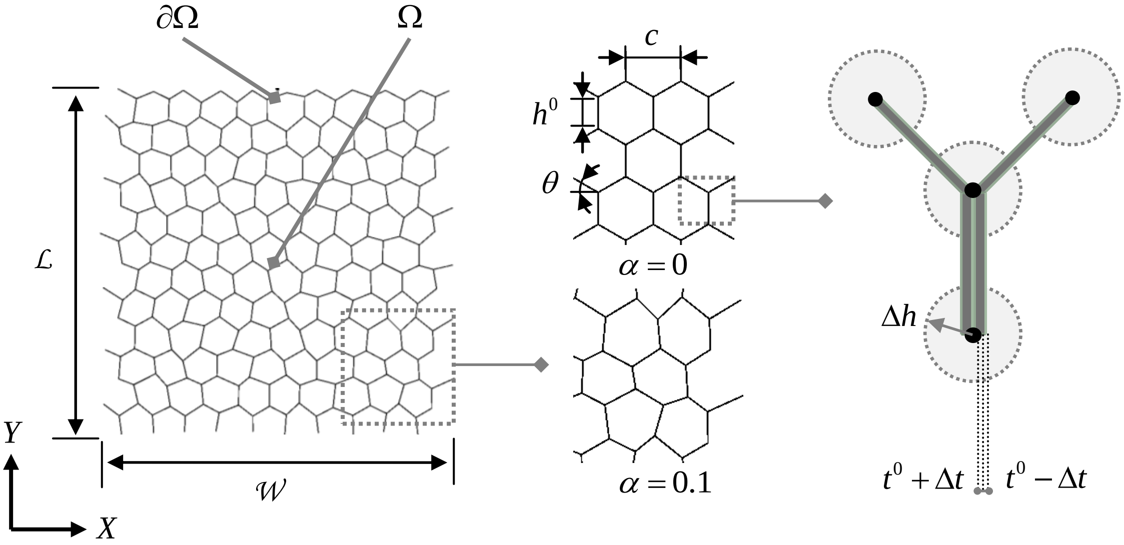

Figure 5: Schematic representation of honeycomb material geometry.

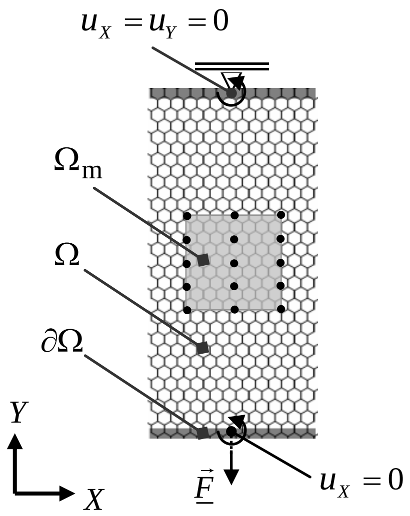

Figure 6: Schematic representation of the loading and boundary conditions, and the domains used in the simulation experiments. Here, u_X and u_Y are the displacement components in the directions of X- and Y-axes, respectively.

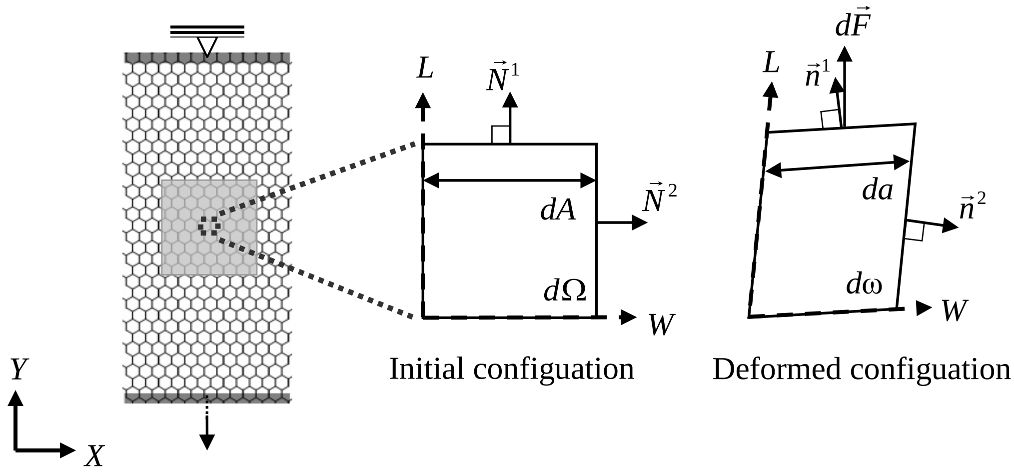

Figure 7: Infinitesimal material element in initial (left) and deformed (right) configurations. Here, $d\Omega$, dA represent the infinitesimal domain and unit surface area in the initial configuration, respectively, while $d\omega$, da are for the same parameters in the deformed configuration. Surface normal vectors are denoted with $\vec{N}^i$ and $\vec{n}^i$, for which $i \in \{1, 2\}$.

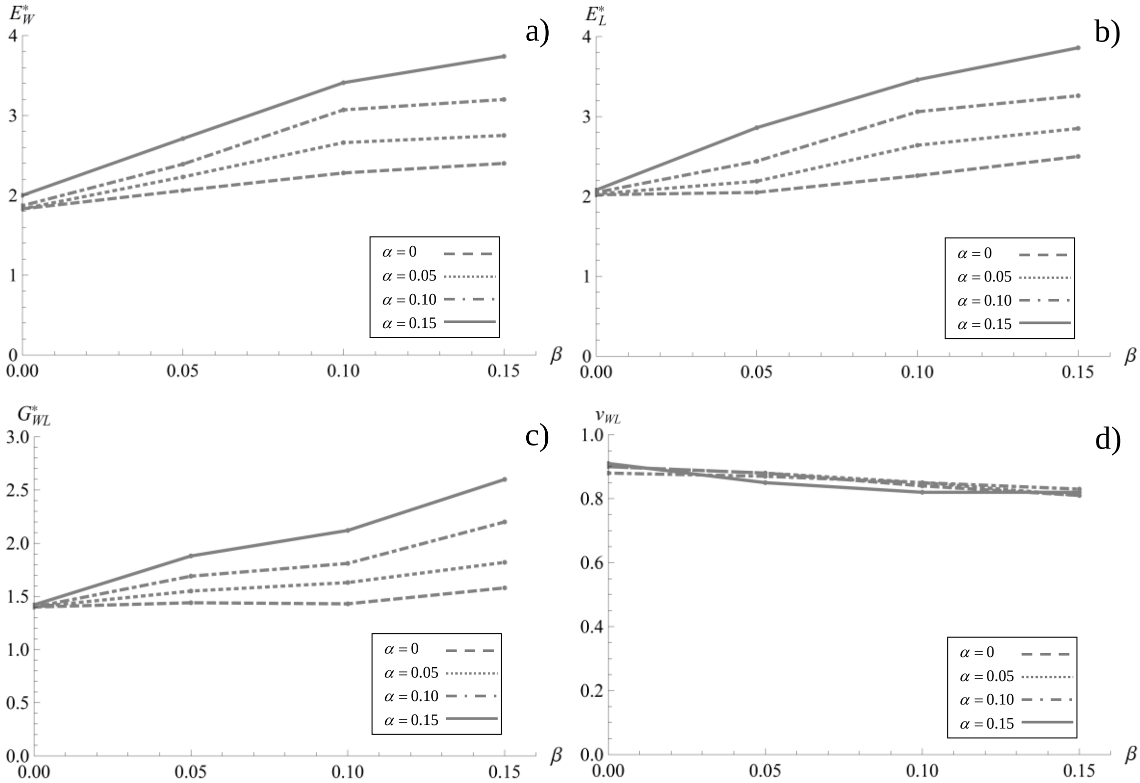

Figure 8: Effect of cell wall thickness variations on the non-dimensional effective in-plane elastic properties: a) E_W^* versus β, b) E_L^* versus β, c) G_{WL}^* versus β, and d) v_{WL} versus β.

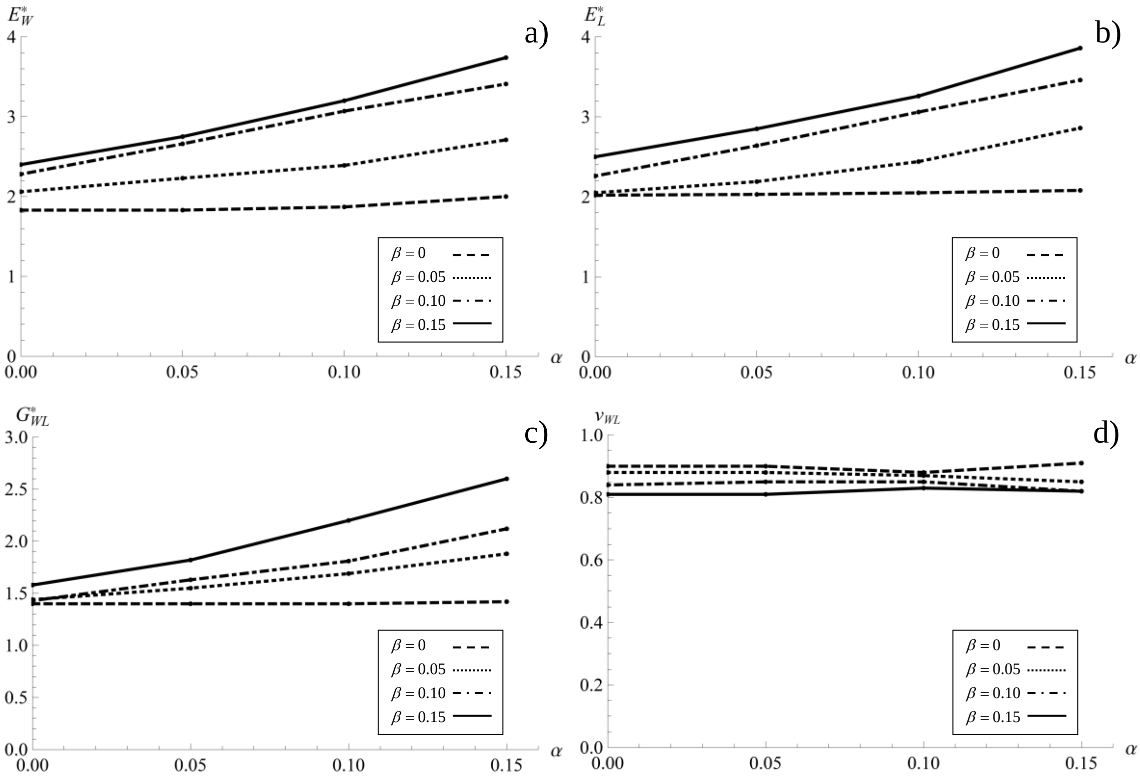

Figure 9: Effect of cell wall height variations on the non-dimensional effective in-plane elastic properties: a) E_W^* versus α, b) E_L^* versus α, c) G_{WL}^* versus α, and d) v_{WL} versus α.

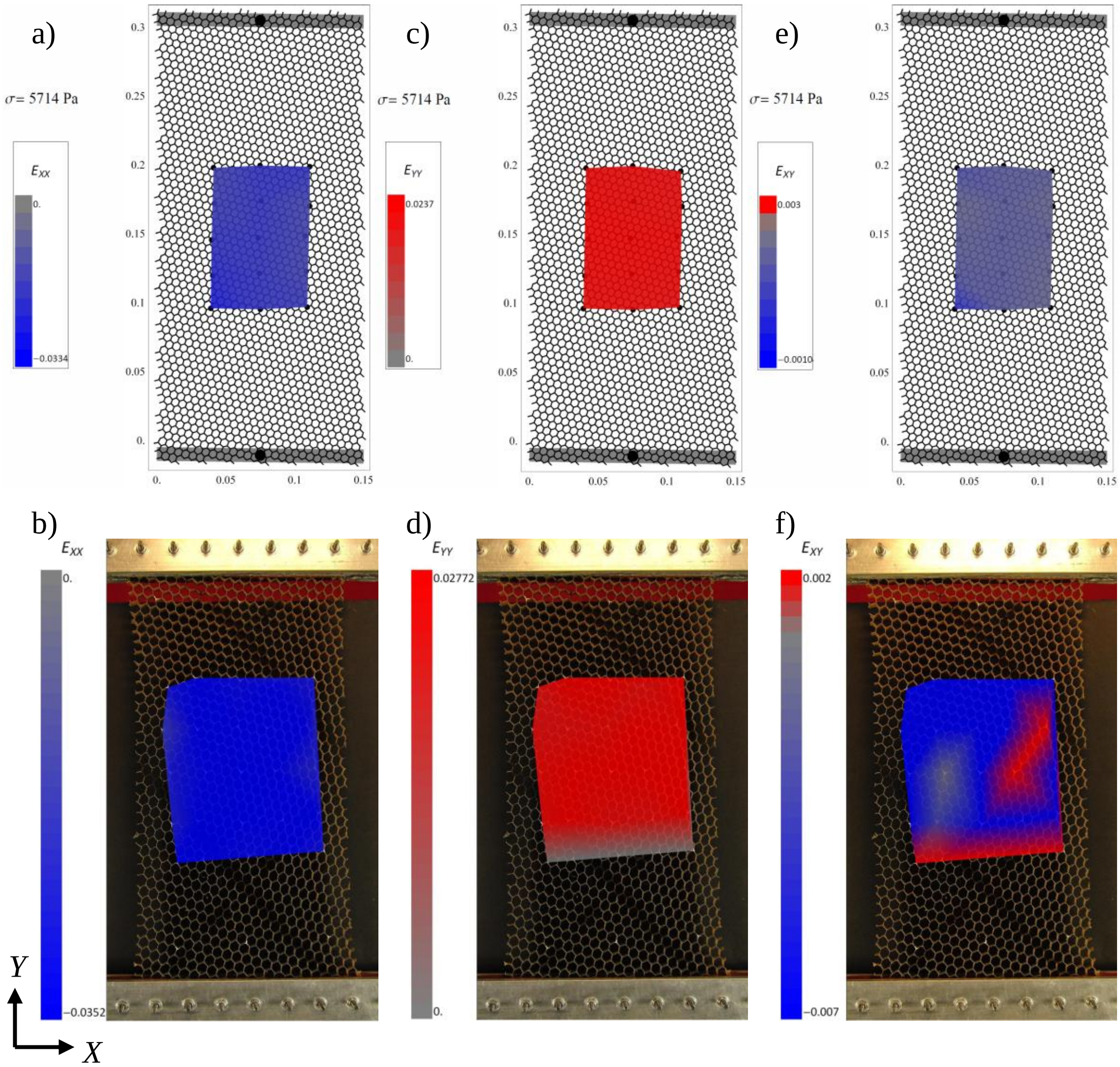

Figure 10: Comparison between the strain fields obtained through the physical and simulation experiments for Nomex® honeycomb specimen with $c = 6$ mm, $\mathcal{T} = 7$ mm and $\varphi = 45^{\circ}$ under uni-axial tensile load $\underline{F}_Y = -6$ N: a) Simulated strain field ε_{XX}, b) Measured strain field ε_{XX}, c) Simulated strain field ε_{YY}, d) Measured strain field ε_{YY}, e) Simulated strain field ε_{XY}, f) Measured strain field ε_{XY}.